FEM Analysis of Current Sharing in REBCO Coated Conductor Cables for Particle Accelerator Applications

S. Xue, M. Majoros, M. D. Sumption, *Senior Member, IEEE*, T. Garg, and E. W. Collings

***Abstract*—Current sharing is an important self-protection mechanism in rare earth barium copper oxide (REBCO) coated conductor (CC) tapes and cables that are intended for the construction of high field magnets. Because of the slower quench propagation rate of such cables, we expect that cooling is also required to facilitate the current sharing. We explored this idea by constructing FEM models that include liquid helium cooling and inter-strand contact properties. The results showed that given metallic inter-strand contact, a three-layer tape stack with a defective central tape could carry at least 3.05 I_c (where I_c is defined for an individual tape). When the inter-strand electrical contact efficiency, η (η = inter-strand contact resistance $*$ contact area), was adjusted to be 5400 $\mu\Omega*cm^2$ and the inter-strand thermal insulance, ω (ω = inter-strand thermal resistance $*$ contact area), was 5.54 $K*m^2/W$, the maximum current that could flow through the defective tape was 0.6 I_c with negligible current sharing to neighboring tapes. After reducing η to 10 $\mu\Omega*cm^2$ and ω to 0.01 $K*m^2/W$ respectively, current sharing to neighboring tapes increased by 800 times, and the hot spot temperature was reduced. However, if the inter-strand thermal contact was insulating, regardless of the value of η, the same tape stack exhibited thermal runaway. Hence, current sharing in REBCO coated conductors is determined by both the inter-strand contact resistance (ICR) and the inter-strand thermal resistance (ITR).**

***Index Terms*—Contact resistance, thermal conductivity, no-insulation coils, HTS cables, HTS magnets.**

I. Introduction

REBCO coated conductors (CCs) are promising material candidates for high field superconducting magnets. Various magnet designs with different cable/tape configurations, such as tape-to-tape no-insulation coils [1], Roebel cables [2], [3], conductor on round core (CORC) cables [4], [5], [6], symmetric tape round REBCO (STAR) cables [7], [8], and twisted stacked tape (TSTC) cables [9] have been proposed and constructed.

Manuscript received 13 November 2022; revised 20 January 2023, 8 February 2023, 19 February 2023, and 25 February 2023; accepted 1 March 2023. Date of publication 7 March 2023; date of current version 27 March 2023. This work was supported by the United States Department of Energy, Office of Science, Division of High Energy Physics under Grant DE SC0011721. *(Corresponding author: S. Xue.)*

The authors are with the Center for Superconducting and Magnetic Materials, Department of Materials Science and Engineering, The Ohio State University, Columbus, OH 43210 USA (e-mail: xue.159@osu.edu).

Color versions of one or more figures in this article are available at https://doi.org/10.1109/TASC.2023.3253666.

Digital Object Identifier 10.1109/TASC.2023.3253666

However, unlike low temperature superconductors such as Nb_3Sn which has a normal zone propagation velocity of 1-100 m/s [10], [11], REBCO CCs have slow normal zone propagation velocities of 3-5 cm/s (driven by their higher T_c) [12], [13]. Hence, one of the biggest challenges for REBCO coated conductor (CC) magnet windings is quench protection against high current density. Quench protection is improved by increasing current sharing between conductors by decreasing the inter-strand contact resistance (ICR) between them. In our previous studies, we have introduced cold pressing, hot pressing, and metal-plating to control the inter-strand electrical contact efficiency, η (η = ICR $*$ contact area), from 5400 $\mu\Omega*cm^2$ down to 2.7 $\mu\Omega*cm^2$ [14], [15], [16]. However, current sharing in REBCO tapes/cables is controlled not only by ICR, but also by the cooling conditions.

It is known that the critical current density (J_c) and the n-value can vary along the length of the REBCO tape [17], [18], [19]. In addition, the tapestar system which has a resolution of $\sim$2 mm has been applied to perform continuous measurements and detection of defects in long REBCO CCs [20], [21], [18], [22]. For a magnet wound with a long length of conductor, drop-outs may be present. When in service, a magnet's cycling may lead to local conductor degradation and localized hot spots. Current sharing to the adjacent layers of the cable can play a critical role in protecting the magnets from quenching. Some interesting work has been performed previously where current sharing behavior has been studied with equivalent circuit models [23], [24]. Our previous study showed that given metallic inter-tape contact properties, a cable containing a defect can still carry its critical current without thermal runaway under some conditions [25]. Similar studies performed on no-insulation coils also demonstrated that ICR is the determinant factor in initiating the self-protection mechanism through current sharing and can affect the maximum operating current in the coil [26]. However, the aforementioned studies failed to explore in detail the effect of cooling, both the heat transfer from the conductor to the ambient and heat transfer within the cables/tapes. Here we describe several different studies based on two models: (1) a single tape conductor and (2) a 3-tape conductor (cable), using various cooling conditions, inter-strand thermal contact resistance (ITR), and ICRs as input parameters. Restricting ourselves to a time independent model, we explore the equilibrium solution for a conductor with imperfect or cyclically damaged strands.

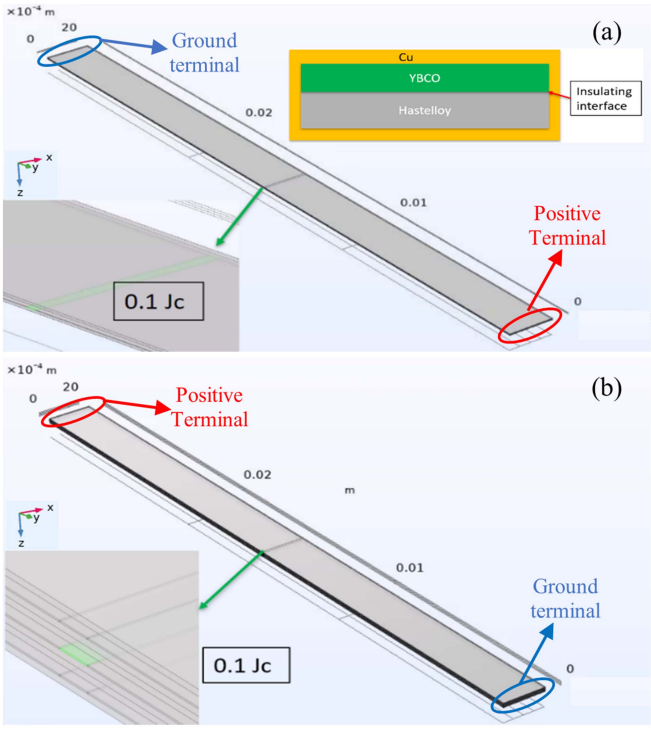

Fig. 1. Geometry of half-tape (a) Single tape model, and (b) Three-tape stack model, with positive and ground injection sites ("terminals") shown. For minimization of computational time, we only modelled the positive-x direction of the tape, assuming the y-z plane to give mirror symmetry.

TABLE I
DETAILS ABOUT TAPES USED IN BOTH MODES

Width of REBCO	4 mm
Thickness of Cu	20 μm (40 μm total)
Thickness of Hastelloy	50 μm
Thickness of REBCO	5 μm
Length of tape	3 cm
Length of defect	0.1 mm
E_C	100 μm/m
n-value	15
I_c (4.2 K,8 T)	596 A
J_c (4.2 K,8 T)	$2.98*10^{10}$ A/m^2

II. MODELING DETAILS

For the single tape model, we assumed a total length of 3 cm, with a pre-existing defect in the middle of the tape. Defects of various sizes, ranging from 0.01 mm to 2 mm, in REBCO CCs have been measured and studied [22], [27]. In this study, we assumed the defect had a length of 0.1 mm, across the entire tape width, and with a current ampacity of 0.1 J_c (Fig. 1). The 20 μm of copper stabilizer was considered to be on both the top and bottom wide surfaces (i.e., 40 μm total) and on the side surfaces. More details are presented in Table I.

A three-tape model "cable" was constructed by sandwiching one tape (with one small central defect) between two tapes without defect.

ComsolMultiphysics was used for FEM numerical modelling of the temperature and current distributions in the models. For

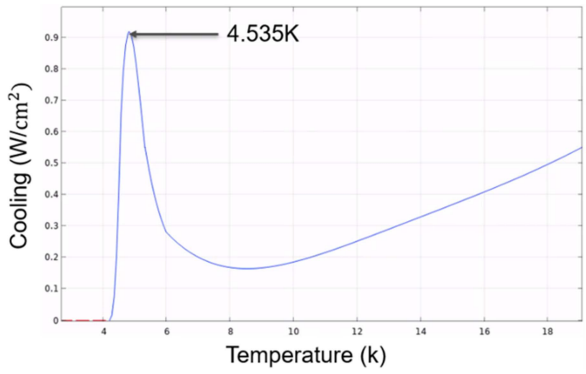

Fig. 2. Liquid helium cooling curve [29], [32].

both the single-tape model and three-tape model, the wide surface of the tape was in the x-y plane, the conductor cross section was in the x-z plane, and a mirror symmetry plane was assumed in the y-z plane at the half width of the conductor [25], [28], this allowed us to reduce computational time by one half (we calculated current distributions on the positive x-direction of the tape only and assumed symmetry, as shown in Fig. 1). The width, length, and thickness of the conductor were along the x-axis, y-axis, and z-axis respectively. To capture the properties of the buffer layers, we set the interface between REBCO layer and the Hastelloy to be insulating. Voltages were applied at the ends of the conductors (the conductor "terminals"), as circled in Fig. 1, with one end corresponding to a positive voltage (current injection site) and with the other end of the conductor, to a "ground", and the current flowed from the positive terminal to the ground.

In this work, we assumed that the conductors were immersed in liquid helium, cooling the conductor's surface. In the longitudinal direction, heat transfer was governed by the thermal conductivity of the respective materials, REBCO, Hastelloy and copper, and the terminal surfaces (the cross section of the ends of the conductor) were defined to be electrically conducting but thermally insulating. The thermal conductivity of the Hastelloy, copper, and REBCO were obtained from Ref. [28], [29], and [30] respectively. The electrical conductivity of Hastelloy and copper were obtained from Ref. [28] and [31]. Based on Ref. [29] and [32], we used the cooling curve shown in Fig. 2. Cooling from nucleate boiling peaks at 4.54 K, followed by a transition to film boiling and a significant decrease in cooling power and heat transfer. Different values of the inter-strand electrical contact efficiency, η (η = inter-strand contact resistance $*$ contact area), and inter-strand thermal insulance, ω (ω = inter-strand thermal resistance $*$ contact area), were used as input parameters to define contact properties, ICR and ITR. In addition, the temperature dependence of J_c was taken into account, this led to an electrical conductivity for the REBCO as defined in (1). We performed a steady-state simulation to capture the final current distribution and temperature profile in each model.

$$J = \sigma E \; ; \; \frac{E}{E_C} = \left(\frac{J}{J_C}\right)^n \; ; \; J_C = J_{C0}\left(1 - \frac{T}{T_C}\right)$$

$$\sigma = J_{C0}\left(1-\frac{T}{T_C}\right)\left(\frac{1}{E_C}\right)^{\frac{1}{n}} E^{\left(\frac{1}{n}-1\right)} \quad (1)$$

III. Results and Discussions

A. Model 1: Single Tape Model

In a real physical scenario, a power supply can operate in either voltage control mode or current control mode. However, in either mode, in actuality the power supply accomplishes this task by manipulating the voltage drop (potential) across the sample. Thus, to model a scenario similar to the physical case where a power supply attempts to maintain a fixed current through a conductor (a power supply in current control mode), we defined the cross sectional surface of the entire tape end (including YBCO, buffer layers, substrate, and stabilizer), circled in Fig. 1(a), to be an equipotential surface. There was one such equipotential surface at the positive terminal, and another at the ground, and the voltage drop across the tape (positive terminal to ground) was set by the (FEM) program to result in a given current (and thus current density) through the tape. In this manner we ran simulations at a series of defined current densities ranging from 0.5 J_c to 0.96 J_c, with the simulation showing the resulting distribution of current density and temperature throughout the sample (tape) at each value of current density. Our goal was to see, for a given set of electrical and thermal condition, at what current density thermal runaway would occur.

As noted above, the defect (0.1 mm long) had a critical current density of 10% of J_c, and the tape was immersed in liquid helium. The current density limit was 0.95 J_c, i.e., above 0.95 J_c, the tape exhibited thermal runaway. The current distribution and temperature profile of the single tape model at $J = 0.95\ J_c$ are presented in Fig. 3. As indicated by the red arrows in Fig. 3(a), current was carried by the REBCO layer before and after the defect (i.e., at value along the y-axis closer to the positive or negative end of the tape), while this current redistributed into the top copper stabilizer at y-positions near the defect region. The highest temperature of the tape was found near the defect, and was 4.6 K; near here the current was redistributed into the copper stabilizer. The power dissipated in the defect due to resistive heating was 4.824 mW. We see that the tape could carry 95% of the nominal J_c with minimal ΔT. Near the defect, the current was shared into the matrix, and some local temperature rise was seen. Nevertheless, even with a spatially small defect with only 10% of the nominal J_c, the excellent liquid cooling enabled minimal temperature rise.

B. Model 2: Three-Tape Model (no Contact Resistance)

The first three-tape model assumed zero inter-strand electrical and thermal contact resistance. The defect (0.1 J_c, where J_c is single tape J_c, and 0.1 mm long) is present in the central tape only. In an approach similar to that for the single tape, for the three-tape stacks, the cross sectional area of the ends of the three tapes, at for example the positive terminal, were set to be at one equipotential, and the cross section of the ends of the three tapes at the ground side of the cable were set to a second equipotential

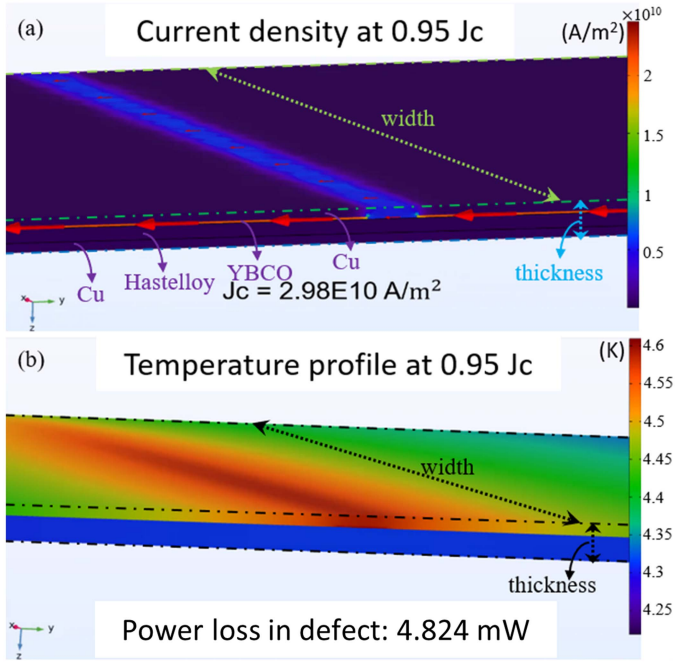

Fig. 3. Model 1: Single tape model (a) Current profile (red arrows indicate the direction of current flow and relative magnitude of current density). Note that we are looking at the y-z plane where the symmetry plane is inserted and the top surface x-y plane. The tape length along y, width along x, and thickness along z. The defect is in the REBCO layer at a particular value of y. (b) Temperature profile.

(zero in this case). Again, the whole of the tape (and cable) cross section was set to these equipotentials, including REBCO, buffer layers, substrate, and stabilizer. The voltage drop across the cable was chosen to achieve a set current density of 3.05 I_c. As presented in Fig 4(a) and (c), the current density in each tape changes along the length of the cable, as we might expect in the presence of a defect. At the positive terminal end of the cable, the top and bottom tapes carried 1.05 I_c, with the middle tape carrying 0.95 I_c and currents were carried by the REBCO layer within each tape. As we travel towards the defect, the current in the REBCO layer of themiddle tape was redistributed away from the defect, into the top and bottom tapes as well as a small amount into the copper stabilizer. Halfway between the two terminals (the longitudinal location of the defect), the current density in the REBCO layer of the top and bottom tapes became 1.28 I_c (of the tape), while the current density in the REBCO layer of the central tape was 0.16 I_c. Here I_c always refers to single tape I_c for the undamaged tape. The result was consistent with our previous study [27]. Moreover, from the temperature profile, Fig. 4(b), the temperature at the defective spot was near 4.37 K, which was still below the nucleate boiling peak temperature. Hence, even 3.05 I_c does not appear to be the limiting current. Compared with Model 1, given two additional neighboring tapes, a defective cable (3-layer tape stack) can carry a current density (3.05 I_c) that is greater than the nominal critical current density (3 I_c), while a single defective tape can only carry 0.95 I_c. In addition, because the current in the middle defective tape can be shared into its neighboring tapes, the power dissipated in the defect due to joule heating is reduced.

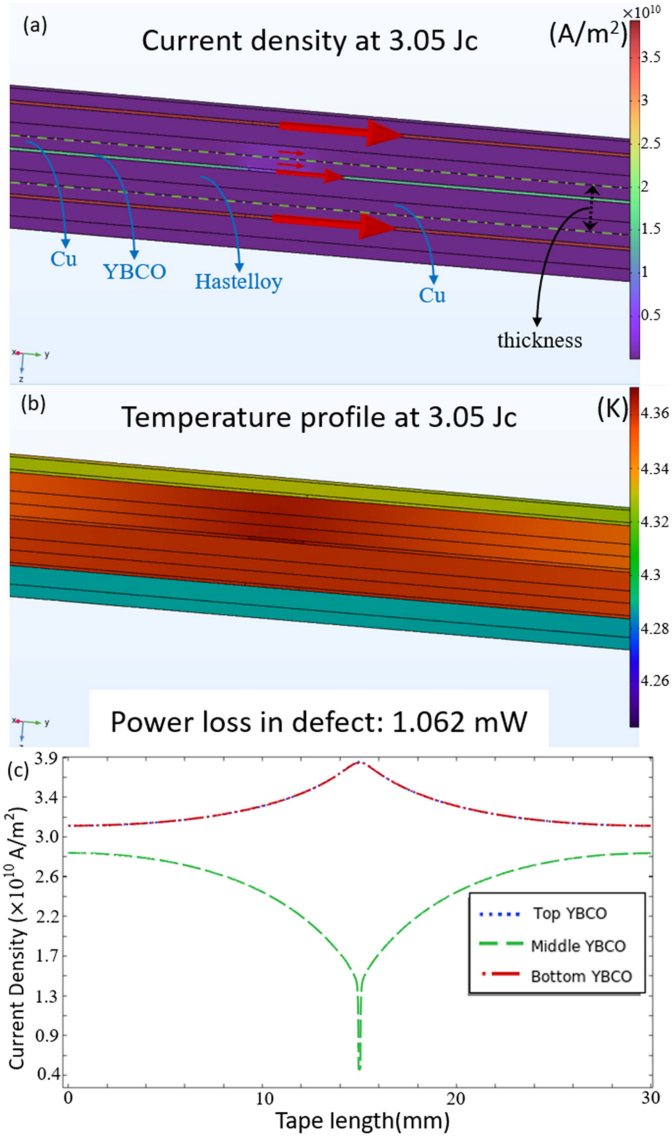

Fig. 4. Model 2: Three-tape stack model (no contact resistance) and we are looking at y-z plane (the middle tape is marked by the two green dashed line); (a) Current profile (red arrows indicate the direction of current flow and relative magnitude of current density), (b) Temperature profile, (c) Current distribution in the REBCO layers along tape length.

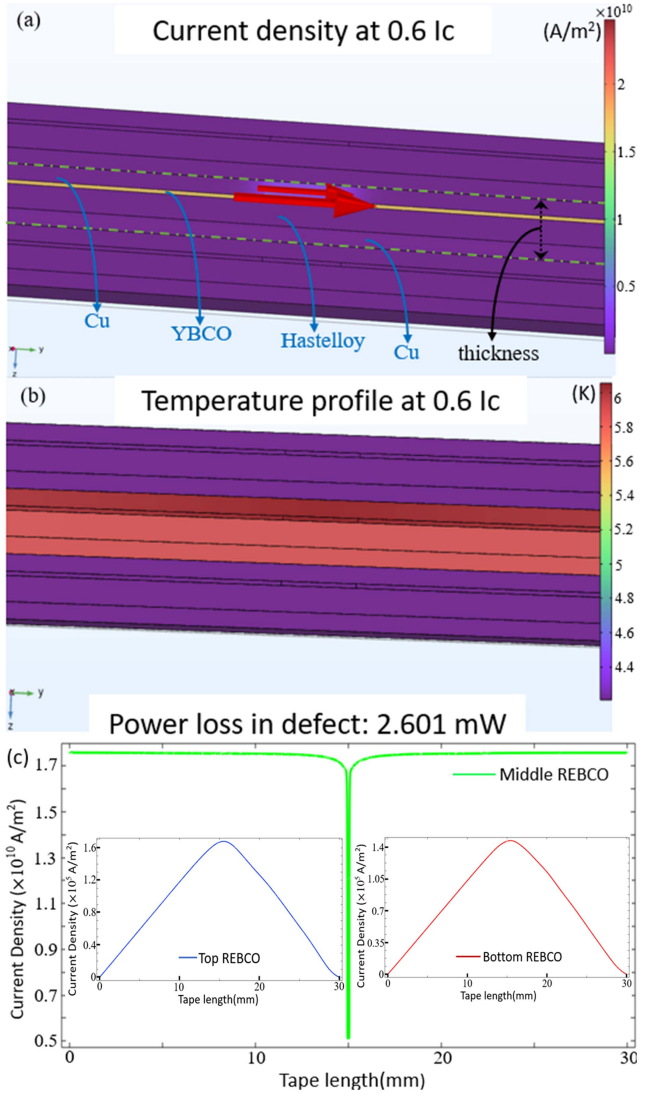

Fig. 5. Model 2.1: Three-tape stack model and we are looking at yz plane (η = 5400 μΩ∗cm^2, ω = 5.54 K∗m^2/W) (the middle tape is marked by the two green dashed line); (a) Current profile (red arrows indicate the direction of current flow and relative magnitude of current density), (b) Temperature profile, (c) Current distribution in the REBCO layers along tape length.

C. *Model 2.1: Three-Tape Model (η = 5400 μΩ∗cm^2, ω = 5.54 K∗m^2/W)*

In Model 2.1, η (η = ICR ∗ contact area), was set at 5400 μΩ∗cm^2 [15]. We assumed that the thickness of the native oxide on the copper surface is 4 nm, and calculated a resistivity based on η. Then we calculated the ratio between the η-based resistivity and the resistivity of copper, and used the same ratio to conclude that the inter-strand thermal insulance, ω (ω = ITR ∗ contact area), was 5.54 K∗m^2/W.

Some models have demonstrated that at steady-state condition, current sharing was determined by the termination resistances [33], [34], [35], [36], [37]. Therefore, to better capture the essence of current sharing around a defect, we ran a simulation where we only "applied current" to the middle tape (the one with the defect); more precisely we defined the positive terminal equipotential to only be on the cross section of the end of the central tape (the one with the defect), and the ground terminal was defined only at the other end of the central tape (REBCO layer, buffer, substrate, and stabilizer). The central tape was in electrical and thermal contact (with defined interfacial values) with both the tapes above and below it via the tape surfaces, but not the ends.

The voltage drop across the cable was chosen to achieve set currents of up to 0.6 I_c (single tape I_c) flowing in the cable. The current redistributed as it neared the middle point between the terminations (near the defect); here the REBCO layer of the central tape only carried 0.17 I_c. The maximum temperature at the defect was 6 K (Fig. 5(b)). The current was redistributed around the defect mainly into the copper stabilizer. As demonstrated in Fig. 5(c), due to the high ICR and ITR, the

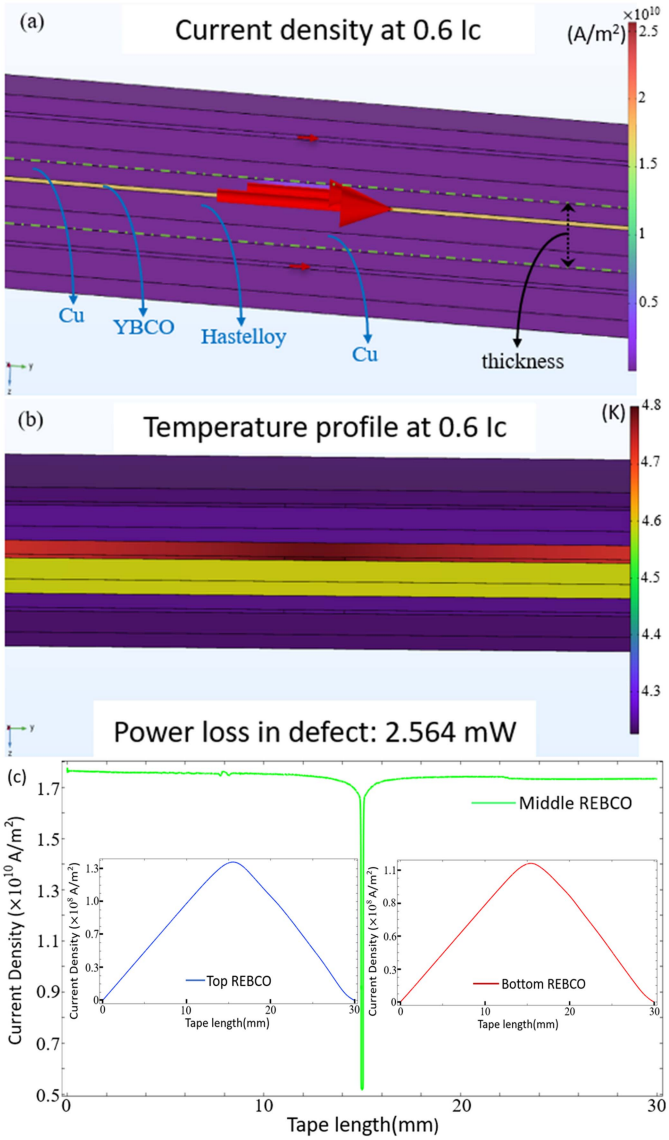

Fig. 6. Model 2.2: Three-tape stack model and we are looking at yz plane ($\eta = 10\ \mu\Omega{*}cm^2, \omega = 0.01\ K{*}m^2/W$) the middle tape is marked by the two green dashed line); (a) Current profile (red arrows indicate the direction of current flow and relative magnitude of current density), (b) Temperature profile. (c) Current distribution along tape length.

REBCO layer in the lower and upper tapes carried only a small amount of the redistributed current, $5{*}10^{-6}\ I_c$ ($1.5{*}10^5$ A/m^2) in each tape, and the majority of the current was shared into the Cu stabilizer. As the current bypassed the defect, the redistributed current in the Cu stabilizer and the REBCO layers of the top and bottom tapes went back into the REBCO layer of the middle tape, and transported to the ground terminal via the lest resistive path.

In this case, a high inter-strand electrical contact resistance (ICR) and inter-strand thermal contact resistance (ITR) kept the level of current sharing small. In comparison with model 1, as a result of reduced cooling and minimal current sharing, the maximum allowed power dissipated in the defect (2.601 mW) of the 3-tape cable is smaller than that in the single tape.

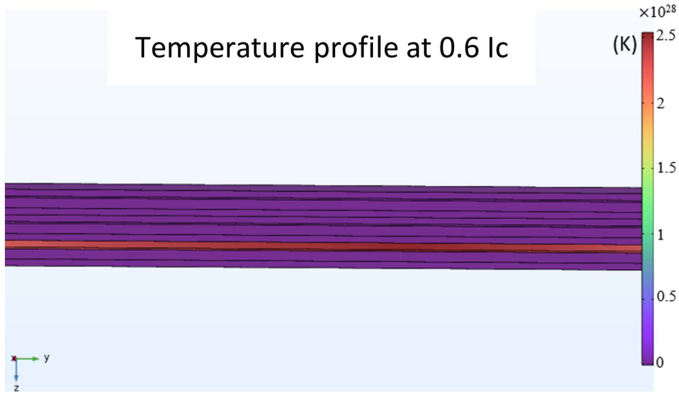

Fig. 7. Temperature profile of Model 2.3: Three-tape stack model (η =5400 $\mu\Omega{*}cm^2$ and insulating thermal contact) and we are looking at yz plane.

D. Model 2.2: Three-Tape Model ($\eta = 10\ \mu\Omega{*}cm^2$, $\omega = 0.01\ K{*}m^2/W$)

In contrast to Model 2 (metallic contact) and Model 2.1 (High ICR and ITR), model 4 has low ICR and ITR. We assumed an η of 10 $\mu\Omega{*}cm^2$ [14] and used the same method as described in Model 2.1 to calculate the inter-strand thermal insulance, ω, which turned out to be 0.01 K$*$m^2/W.

As shown in Fig. 6(b), compared to Model 2.1, given the same current input (0.6 *Ic* of one tape), due to reduced ICR and ITR, the maximum temperature at the defect spot decreased from 6 K to 4.8 K, and the power dissipated in the defect (2.564 mW) also decreased. Based on the current profile, Fig. 6(a) and (c), a current of 0.004 I_c ($J_c = 1.2{*}10^8$ A/m^2) became redistributed to each of the REBCO layer of the upper and lower tapes. After the defect, current redistributed into the adjacent tapes went back to the REBCO layer of the middle tape, because only the cross section surface of the end of the middle tape was set to be the equipotential ground terminal and the REBCO layer was the lest resistive path for current transferring through the tape. The current sharing to the adjacent REBCO CC tapes increased about 800 times due to the reduction of ICR and ITR. In addition, 0.6 I_c is apparently not the limiting current in this three-strand cable, given the lower temperature and reduced power loss in the defect.

E. Model 2.3: Three-Tape Model ($\eta = 5400\ \mu\Omega{*}cm^2$ and Insulating Thermal Contact)

To further demonstrate the significance of inter-strand thermal contact to current sharing and quench prevention, we made Model 2.3, which had the same η as Model 2.1 (η = 5400 $\mu\Omega{*}cm^2$) but an insulating inter-strand thermal contact. We used the same current as in Model 2.1 (0.7 I_c of one tape). As presented in Fig. 7, the insulating thermal contact led to a thermal runaway. Clearly, ITR as well as ICR are needed to define the level of current sharing in this quasistatic condition.

F. Model 2.4: Three-Tape Model ($\eta = 10\ \mu\Omega{*}cm2$, and Insulating Thermal Contact)

Model 2.4 was made by setting η to be the same as Model 2.2 (η = 10 $\mu\Omega{*}cm^2$), but with insulating inter-strand thermal

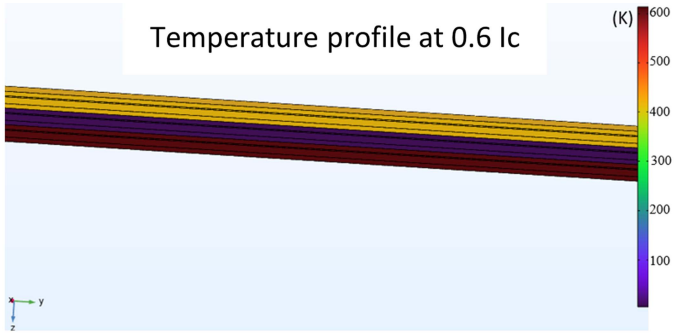

Fig. 8. Temperature profile of Model 2.4 and we are looking at yz plane: Three-tape stack model (ICR = 10 μΩ∗cm^2, and insulating thermal contact).

contact. The simulation result, Fig. 8, showed that regardless of the reduced η, thermal runaway still happened in this scenario as a result of insulating inter-strand thermal contact.

Comparing the five different scenarios simulated with the three-tape model, we can conclude that the allowable cable current density before thermal runaway is determined both by ICR as well as the cooling condition and inter-tape contact properties. Reduction in ITR leads to a bigger margin of energy dissipation in a local defect, while reduced ICR can result in smaller energy dissipation in a local defect. A resistive inter-strand contact and reduced cooling power, such as conduction cooling versus liquid cooling would lead to a lower *Jc* of a cable.

IV. Conclusion

In this study, we investigated the limiting factors to current sharing in REBCO CC tape stacks/ cables by performing FEM analysis for six different scenarios with two models, single tape model, three-tape stack with zero contact resistance, three-tape stack given $\eta = 5400$ μΩ∗cm^2 and $\omega = 5.54$ K∗m^2/W, three-tape stack given $\eta = 10$ μΩ∗cm^2 and $\omega = 0.01$ K∗m^2/W, three-tape stack given $\eta = 5400$ μΩ∗cm^2 and insulating inter-strand thermal contact, and three-tape stack given $\eta = 10$ μΩ∗cm^2 and insulating inter-strand thermal contact. We concluded that both the cooling condition and inter-strand contact properties were determining factors for current sharing. Further efforts are required to understand the systematics of the behavior, and to potentially formulate an analytical expression to describe this phenomenon.

References

[1] H. S, K. Kim, K. Kim, and X. Hu, "45.5-tesla direct-current magnetic field generated with a high-temperature superconducting magnet," *Nature*, vol. 570, pp. 496–499, Jun. 2019.

[2] J. Fleiter, C. Lorin, and A. Ballarino, "On Roebel cable geometry for accelerator magnet," *IEEE Trans. Appl. Supercond.*, vol. 26, no. 3, Apr. 2016, Art. no. 4802805.

[3] G. A. Kirby et al., "First cold powering test of REBCO Roebel wound coil for the EuCARD2 future magnet development project," *IEEE Trans. Appl. Supercond.*, vol. 27, no. 4, Jun. 2017, Art. no. 4003307.

[4] D. C. van der Laan, J. D. Weiss, and D. M. McRae, "Status of CORC® cables and wires for use in high-field magnets and power systems a decade after their introduction," *Supercond. Sci. Technol.*, vol. 32, Feb. 2019, Art. no. 033001.

[5] D. C. van der Laan et al., "A CORC® cable insert solenoid: The first high-temerature superconducting insert magnet tested at currents exceeding 4 kA in 14 T background magnet field," *Supercond. Sci. Technol.*, vol. 33, no. 5, Apr. 2020, Art. no. 05LT03.

[6] X. Wang et al., "Development and performance of a 2.9 Tesla dipole magnet using high-temperature superconductor CORC® wires," *Supercond. Sci. Technol.*, vol. 34, no. 1, Dec. 2020, Art. no. 015012.

[7] S. Kar, W. Luo, A. B. Yahia, X. Li, G. Majkic, and V. Selvamanickam, "Symmetric tape round REBCO wire with Je (4.2 K, 15 T) beyond 450 A mm−2 at 15 mm bend radius: A viable candidate for future compact accelerator magnet applications," *Supercond. Sci. Technol.*, vol. 31, Mar. 2018, Art. no. 04LT01.

[8] S. Kar et al., "Next-generation highly flexible round REBCO STAR wires with over 580 A mm^{-2} at 4.2 K, 20 T for future compact magnets," *Supercond. Sci. Technol.*, vol. 32, no. 10, Aug. 2019, Art. no. 10LT01.

[9] M. Takayasu, L. Chiesa, L. Bromberg, and J. V. Minervini, "HTS twisted stacked-tape cable conductor," *Supercond. Sci. Technol.*, vol. 25, Dec. 2011, Art. no. 014011.

[10] S. Murase et al., "Normal zone and quench characteristics of Nb_3Sn wires with jelly-roll and in-situ processed CuNb reinforcements," *IEEE Trans. Appl. Supercond.*, vol. 11, no. 1, pp. 3627–3630, Mar. 2001.

[11] A. den Ouden et al., "Normal zone propagation in high-current density Nb_3Sn conductors for accelerator magnets," *IEEE Trans. Appl. Supercond.*, vol. 14, no. 2, pp. 279–282, Jun. 2004.

[12] S. Liu, L. Ren, J. Li, and Y. Tang, "Analysis of quench propagation characteristics of the YBCO coated conductor," *Phys. C Supercond. Appl.*, vol. 471, no. 21/22, pp. 1080–1082, Nov. 2011.

[13] H. Chen, H.-J. Liu, F. Liu, and Y. Shi, "Development of a normal zone propagation insert set-up for YBCO superconducting tape," *IEEE Trans. Appl. Supercond.*, vol. 31, no. 8, Nov. 2021, Art. no. 9001004.

[14] S. Xue et al., "Electrical contact resistance in the REBCO stacks and cables with modified surface," *IEEE Trans. Appl. Supercond.*, vol. 32, no. 6, Sep. 2022, Art no. 4802506.

[15] S. Xue, M. Sumption, and E. Collings, "YBCO coated conductor interlayer electrical contact resistance measured from 77 K to 4 K under applied pressure up to 9.4 MPa," *IEEE Trans. Appl. Supercond.*, vol. 31, no. 5, Aug. 2021, Art. no. 7000305.

[16] C. J. Kovacs, M. D. Sumption, M. Majoros, and E. W. Collings, "Modified interconductor contact resistivity in coated conductor stacks and Roebel cables," *IEEE Trans. Appl. Supercond.*, vol. 30, no. 4, Jun. 2020, Art. no. 6600505.

[17] V. Pothavajhala, C. H. Kim, L. Graber, and S. Pamidi, "Effects of longitudinal variations in critical current and n-value of individual tapes on the performance of superconducting cables," *IEEE Trans. Appl. Supercond.*, vol. 25, no. 3, Jun. 2015, Art. no. 5400604.

[18] J. J. Gannon, A. P. Malozemoff, R. C. Diehl, P. Antaya, and A. Mori, "Effect of length scale on critical current measurement in high temperature superconductor wires," *IEEE Trans. Appl. Supercond.*, vol. 23, no. 3, Jun. 2013, Art. no. 8002005.

[19] J.-H. Kim, C. H. Kim, V. Pothavajhala, and S. V. Pamidi, "Current sharin and redistribution in superconducting DC cable," *IEEE Trans. Appl. Supercond.*, vol. 23, no. 3, Jun. 2013, Art. no. 4801304.

[20] THEVA Dünnschichttechnik GmbH, Ismaning, Germany.

[21] S. Furtner, R. Nemetschek, R. Semerad, G. Sigl, and W. Prusseit, "Reel-to-reel critical current measurement of coated conductors," *Supercond. Sci. Technol.*, vol. 17, no. 5, pp. S281–S284, Mar. 2004.

[22] A. Molodyk et al., "Development and large volume production of extremely high current density YBa_2Cu_{3O7} superconducting wires for fusion," *Sci. Rep.*, vol. 11, Jan. 2021, Art. no. 2084.

[23] Z. Bai, W. Zu, C. Chen, and X. Zheng, "Modeling and numerical analysis of resistance network for non-insulated superconducting magnet," *Cryogenics*, vol. 60, pp. 19–23, Jan. 2014.

[24] A. C. A. Martínez, Q. Ji, S. O. Prestemon, X. Wang, and G. H. I. M. Cuna, "An electric-circuit model on the inter-tape contact resistance and current sharing for REBCO cable and magnet applications," *IEEE Trans. Appl. Supercond.*, vol. 30, no. 4, Jun. 2020, Art. no. 6600605.

[25] M. Majoros, M. D. Sumption, S. Xue, and E. W. Collings, "Stability and current sharing in YBCO cables-impact of broken elements - FEM modeling," *IEEE Trans. Appl. Supercond.*, vol. 32, no. 6, Sep. 2022, Art. no. 8200705.

[26] Y. Yanagisawa et al., "Basic mechanism of self-healing from the thermal runaway for uninsulated REBCO pancake coils," *Phys. C Supercond. Appl.*, vol. 499, pp. 40–44, Apr. 2014.

[27] M. Polak, P. N. Barnes, P. Mozola, and G. A. Levin, "Critical current in YBCO coated conductors in the presence of a macroscopic defect," *IEEE Trans. Appl. Supercond.*, vol. 19, no. 3, pp. 2921–2924, Jun. 2009.
[28] https://www.comsol.com
[29] A. D. Berger, *Stability of Superconducting Cables With Twisted Stacked YBCO Coated Conductors*. Cambridge, MA, USA: MIT Plasma Science and Fusion Center, Feb. 2012, pp. 28–30.
[30] G. Grissonnanche et al., "Direct measurement of the upper critical field in cuprate superconductors," *Nature Commun.*, vol. 5, Feb. 2014, Art. no. 3280.
[31] J. W. Ekin, *Experimental Techniques for Low-Temperature Measurements*. London, U.K.: Oxford Univ. Press, Oct. 2006, pp. 241–248.
[32] E. G. Brentari, P. J. Giarratano, and R. V. Smith, "Boiling heat transfer for oxygen, nitrogen, hydrogen, and helium," National Bureau of Standards, p. 5, Sep. 1965.
[33] M. Majoros, M. D. Sumption, S. Xue, and E. W. Collings, "Modeling of thermal effect during current sharing in YBCO cables containing broken elements and other defects–FEM modeling," *IEEE Trans. Appl. Supercond.*, to be published.
[34] M. Takayasu, L. Chiesa, N. C. Allen, and J. V. Minervini, "Present status and recent developments of the twisted stacked-tape cable conductor," *IEEE Trans. Appl. Supercond.*, vol. 26, no. 2, Mar. 2016, Art. no. 6400210.
[35] G. P. Willering, D. C. van der Laan, H. W. Weijers, P. D. Noyes, G. E. Miller, and Y. Viouchkov, "Effect of variations in terminal contact resistances on the current distribution in high-temperature superconducting cables," *Supercond. Sci. Technol.*, vol. 28, Jan. 2015, Art. no. 035001.
[36] L. Bromberg, M. Takayasu, P. Michael, J. V. Minervini, and A. Dietz, "Current distribution and re-distribution in HTS cables made from 2nd generation tapes," in *Proc. Amer. Inst. Phys. Conf.*, 2012, pp. 1001–1008.
[37] S. Venuturumilli et al., "Forceful uniform current distribution among all the tapes of a coaxial cable to enhance the operational current," *IEEE Trans. Appl. Supercond.*, vol. 27, no. 4, Jun. 2017, Art. no. 4801904.